Published February 1, 1991

Sodium and Calcium Currents in Dispersed Mammalian Septal Neurons

ANTONIO CASTELLANO and JOSÉ LÓPEZ-BARNEO

From the Departamento de Fisiología y Biofísica, Facultad de Medicina, 41009 Sevilla, Spain

ABSTRACT Voltage-gated Na^+ and Ca^{2+} conductances of freshly dissociated septal neurons were studied in the whole-cell configuration of the patch-clamp technique. All cells exhibited a large Na^+ current with characteristic fast activation and inactivation time courses. Half-time to peak current at −20 mV was 0.44 ± 0.18 ms and maximal activation of Na^+ conductance occurred at 0 mV or more positive membrane potentials. The average value was 91 ± 32 nS (~11 mS cm^{-2}). At all membrane voltages inactivation was well fitted by a single exponential that had a time constant of 0.44 ± 0.09 ms at 0 mV. Recovery from inactivation was complete in ~900 ms at −80 mV but in only 50 ms at −120 mV. The decay of Na^+ tail currents had a single time constant that at −80 mV was faster than 100 μs. Depolarization of septal neurons also elicited a Ca^{2+} current that peaked in ~6–8 ms. Maximal peak Ca^{2+} current was obtained at 20 mV, and with 10 mM external Ca^{2+} the amplitude was 0.35 ± 0.22 nA. During a maintained depolarization this current partially inactivated in the course of 200–300 ms. The Ca^{2+} current was due to the activity of two types of conductances with different deactivation kinetics. At −80 mV the closing time constants of slow (SD) and fast (FD) deactivating channels were, respectively, 1.99 ± 0.2 and 0.11 ± 0.03 ms (25°C). The two kinds of channels also differed in their activation voltage, inactivation time course, slope of the conductance–voltage curve, and resistance to intracellular dialysis. The proportion of SD and FD channels varied from cell to cell, which may explain the differential electrophysiological responses of intracellularly recorded septal neurons.

INTRODUCTION

Mammalian central neurons possess intrinsic electrical properties that make them able to generate complex firing patterns. This implies the existence of a variety of membrane ionic conductances which, with a few exceptions, are poorly characterized. Some properties of Na^+ channels have recently been studied in dissociated hippocampal (Sah et al., 1988) and neocortical (Huguenard et al., 1988) neurons, as well as in Purkinje cells of organotypic cerebellar cultures (Gähwiler and Llano, 1989), but additional work is still needed to fully investigate the biophysical properties of cerebral Na^+ channels and to ascertain whether their characteristics are homogeneous in different brain regions. Ca^{2+} channels, on the other hand, have been

Address reprint requests to Dr. J. López-Barneo, Departamento de Fisiologia Médica y Biofísica, Facultad de Medicina, Avda. Sánchez Pizjuán, 4, 41009 Sevilla, Spain.

J. GEN. PHYSIOL. © The Rockefeller University Press · 0022-1295/91/02/0303/18 $2.00
Volume 97 February 1991 303–320

intensively studied in neurons of the peripheral nervous system (Fedulova et al., 1985; Carbone and Lux, 1987; Fox et al., 1987; Swandulla and Armstrong, 1988), but within the brain they have been only partially characterized (Hernández-Cruz and Pape, 1989; Meyers and Barker, 1989). We have previously shown that intracellularly recorded septal neurons in in vitro brain slices display differential electrical responses due to the variability in the distribution of membrane ionic conductances (López-Barneo et al., 1985; Alvarez de Toledo and López-Barneo, 1988). This article continues our preceding work and focuses on the characterization of the ionic currents of freshly dissociated septal neurons from adult guinea pigs. Due to their size and regular geometry these cells provide an excellent preparation for studying the voltage-activated ionic channels in a well-clamped neuronal membrane using the whole-cell variant of the patch-clamp technique (Hamill et al., 1981). This research not only has biophysical interest, it is also of importance because an accurate analysis

TABLE I

Composition of Solutions

	NaCl	KCl	$CaCl_2$	$MgCl_2$	$BaCl_2$	$CoCl_2$	Trizma*	HEPES
External								
130 Na	130	2.7	2.5	1	—	—	—	10
80 Na	80	2.7	2.5	1	—	—	70	—
10 Ca	70	2.7	10	—	—	—	60	—
10 Ba	70	2.7	—	—	10	—	60	—
Mg/Co	70	2.7	1	7.5	—	1.5	60	—

	NaCl	KCl	K-glutamate	KF	$MgCl_2$	CsCl	CsF	HEPES	EGTA
Internal									
130 K	—	30	80	20	2	—	—	10	5
130 Cs	—	—	—	—	2	110	20	10	5
40 Na	40	—	—	—	2	70	20	10	5

All values are given in millimolar.
pH was 7.4 in external and 7.3 to 7.35 in internal solutions
*Tris (hydroxymethyl)aminomethane (pH = 7.4).

of the ionic conductances of central neurons is required before undertaking the investigation of their modulation by neuromodulators and drugs. This article concentrates on the description of the properties of Na^+ and Ca^{2+} currents; the K^+ current is only briefly presented and therefore not studied in detail.

METHODS

Cells were obtained from coronal slices, 300–400 μm thick, of the adult guinea pig septal region. The procedure followed for slicing was the same as previously described (Alvarez de Toledo and López-Barneo, 1988). For cell dissociation, six slices containing only the septal nucleus were placed in a vial with 3 ml of Earle solution (Flow Laboratories, Inc., McLean, VA) containing 0.2 mg/ml of trypsin type IX and 0.05 mg/ml of DNase type II (Sigma Chemical Co., St. Louis, MO). This solution was continuously bubbled with a mixture of 95% O_2 and 5% CO_2 and the tissue was incubated for 20 min at 37°C. After this time period the tissue was washed

twice and the enzymes were removed. Cells were mechanically dispersed using fire-polished Pasteur pipettes, centrifuged, and resuspended in MEM culture medium supplemented with glutamine, antibiotics, and bovine fetal serum. Cells were plated on fragments of glass coverslips treated with poly-L-lysine and maintained in an incubator until use (between 2 and 6 h after plating). The general procedures and the set up used for recording of whole-cell currents were the same as previously described (Ureña et al., 1989*a*). The composition of the recording solutions is given in Table I. Junction potentials were corrected once the electrode was in the bath and immediately before establishing a seal. In the text and in the figure legends solutions are indicated as external//internal. Experiments were performed at room temperature (20–25°C).

For recording we used a patch-clamp amplifier built in our laboratory following the design of Sigworth (1983). A fast and uniform control of the membrane potential was favored by the use of low resistance electrodes (between 0.8 and 2 MΩ), a feedback resistance of only 100 MΩ in the current-to-voltage converter, and electronic compensation of series resistance. With this recording configuration capacity transients typically had time constant values between 40 and 50 μs. Clamp speed was further enhanced by ballistic charging of membrane capacitance (Matteson and Armstrong, 1984). Compensation of series resistance was done empirically; in most experiments we compensated for 1.5 times electrode resistance. An IBM-PC/AT computer interfaced to the analog electronics was used for pulse generation and for acquisition, display, storage, and analysis of the data. The interface and the associated software were developed and fabricated in our laboratory (Ureña et al., 1989*b*) and allowed us subtraction of the linear ionic and capacity currents. Sampling interval was either 10 or 20 μs. Tail currents were fitted with one or the sum of two exponentials using a least-squares procedure.

RESULTS

Cells subjected to voltage-clamp had an almost spherical shape and no appreciable processes under the light microscope. The diameter of the dispersed neurons varied between 12 and 25 μm. Membrane capacitance, calculated from the time integral of the transient capacity currents, was 8 ± 3 pF (mean ± SD, n = 87). Input resistance was 1.5 ± 0.6 GΩ.

Whole-Cell Currents

Fig. 1 *A* is a representative example of the major current components recorded in septal neurons during a step depolarization to 20 mV. At the beginning of the pulse the cell generates a fast inward current that peaks in less than 0.5 ms. In the course of the next 2 ms the current changes from inward to outward and rises slowly until the end of the pulse. On return to the holding potential there is an almost instantaneous jump in the current (which in this recording lasts less than 80 μs) and a large tail current is observed. Fig. 1 *B* shows the current recorded after blockade of K^+ channels by internal Cs^+. The outward current is suppressed, and after the initial fast inward component a second, more steady component is disclosed, which, when the pulse is turned off, is followed by the tail current. External addition of tetrodotoxin (TTX, 0.5–1 μM) abolishes the fast inward current, while the steady component and the tail remain unaltered (Fig. 1 *C*). It will be shown later that both the slow inward current and the tail disappear after removal of external Ca^{2+}. These findings indicate that the different components of the whole-cell current are due to the activity of Na^+, Ca^{2+}, and K^+ channels. The three current components were recorded in every neuron

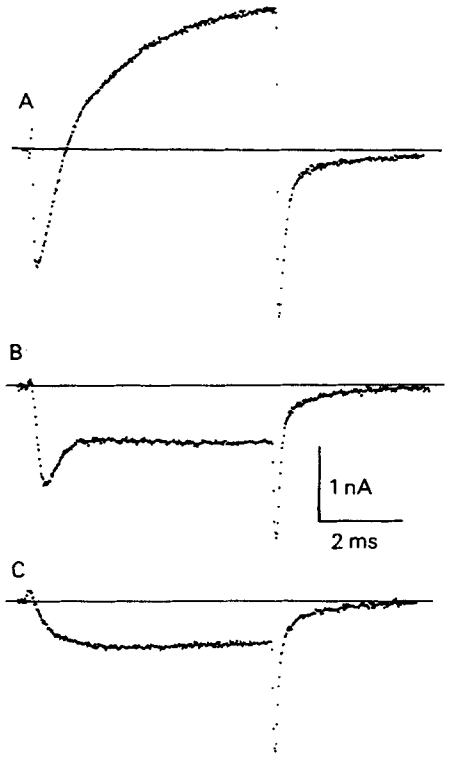

FIGURE 1. Major current components in septal neurons. The three current sweeps were recorded during 6-ms voltage steps to 20 mV from a holding potential of −80 mV. Solutions: 130 Na//130 K (*A*), 10 Ca//130 Cs (*B* and *C*). In *C*, 1 μM TTX was added to the external solution.

studied ($n > 150$), although the amplitude of each varied from cell to cell. In the following sections we analyze the properties of Na^+ and Ca^{2+} currents.

Na^+ Channels

Activation and conductance–voltage relations. Na^+ current was studied in isolation in cells dialyzed with the 130 mM Cs^+ solution and bathed in an external solution with 130 mM Na^+, where 90% of the Ca^{2+} was replaced by Mg^{2+} and Co^{2+} (see Table I). In these solutions depolarization elicited large Na^+ currents that at 0 mV had a peak amplitude of 4.6 ± 1.6 nA ($n = 21$). Assuming no membrane infolding, current density was 0.6 mA cm^{-2}. Most experiments were, however, performed with the 80 Na external solution (Table I) to favor an accurate control of the membrane potential. Fig. 2 illustrates a current trace obtained in low external Na^+. The recording is very representative of a well-controlled Na^+ current with fast activation

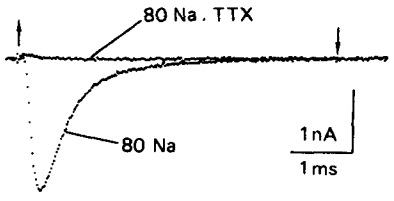

FIGURE 2. Na^+ current recorded on isolation during a voltage pulse from −80 to 0 mV. The arrows indicate the onset and the termination of the pulse. Solutions were 80 Na//130 Cs. The current was completely suppressed by 1 μM TTX.

and complete inactivation in 5–6 ms. The figure also shows that addition of TTX produced a complete blockade of the current. With 80 mM external Na^+, peak current amplitude at 0 mV was 2.8 ± 1.3 nA (n = 49). Good control of the membrane potential was also indicated by a conductance–voltage curve with a sigmoid rising phase (not shown), and because currents of different amplitude recorded at the same membrane potential (as, for instance, those in Fig. 6*A*) had, after scaling, almost identical time courses.

Fig. 3*A* is a family of Na^+ currents generated by depolarization to the indicated membrane potentials. In this experiment we added 40 mM Na^+ to the internal solution to obtain a well-defined reversal potential (E_{Na}). Current is inward at

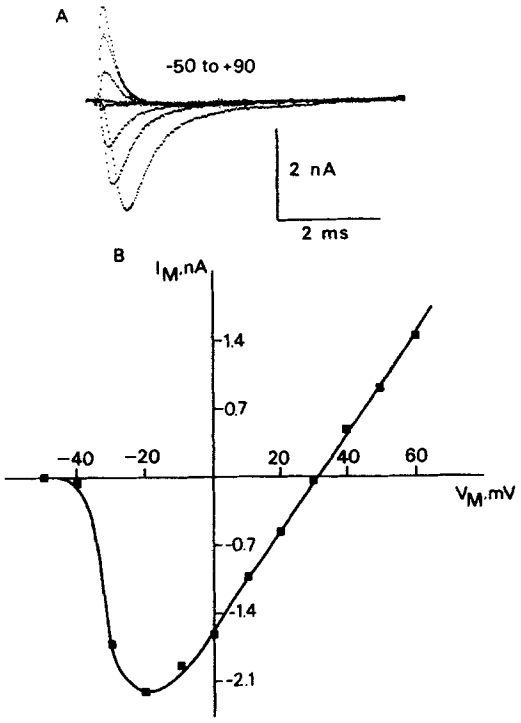

FIGURE 3. Na^+ *I-V* relations. (*A*) Family of current sweeps elicited by depolarizations to −50, −30, −10, 10, 30, 50, 70, and 90 mV from a holding potential of −80 mV. (*B*) Peak current amplitude (ordinate) at various membrane potentials (abscissa). Intersection of the continuous line with the abscissa gives the value of the reversal potential (31 mV). Solutions: 130 Na//40 Na.

membrane potentials more negative than E_{Na} and outward at more positive potentials. The current turns on rapidly and inactivates completely at all voltages. Activation kinetics speed up with membrane depolarization and half-time to peak current is 0.44 ± 0.18 ms at −20 mV but only 0.21 ± 0.06 ms at +20 mV (n = 10). Fig. 3*B* is the *I-V* curve obtained by measuring the peak current at various membrane potentials. This figure shows that a measurable current can be recorded at −50 mV and that the maximal peak current is obtained between −20 and −10 mV. The reversal potential of the current occurs at +31 mV, which is similar to the Na^+ equilibrium potential calculated by the Nernst equation. This suggests that, as in other preparations (Fenwick et al., 1982; Matteson and Armstrong, 1984; Ureña et al., 1989*a*), the aqueous components of the cytosol equilibrate completely with the

pipette solution. Na^+ conductance (g_{Na}), calculated by the formula $g_{Na} = I_{Na}/(V_M - E_{Na})$ (Hodgkin and Huxley, 1952), was maximal at 0 mV or more positive voltages. The average value from four septal neurons was 91 ± 32 nS (~11 mS cm^{-2}), and half of the total conductance was activated at −35 mV.

Inactivation. During a maintained depolarization the inactivation of Na^+ currents could be well fitted by a single exponential function. This is illustrated by the recording of Fig. 4 *A*. In the range between −20 and +60 mV inactivation time constant diminishes with membrane depolarization (Fig. 4 *B*) and at 0 mV it has an average value of 0.44 ± 0.09 ms (n = 5).

The voltage dependence of steady-state inactivation is illustrated in Fig. 5. In *A* it is

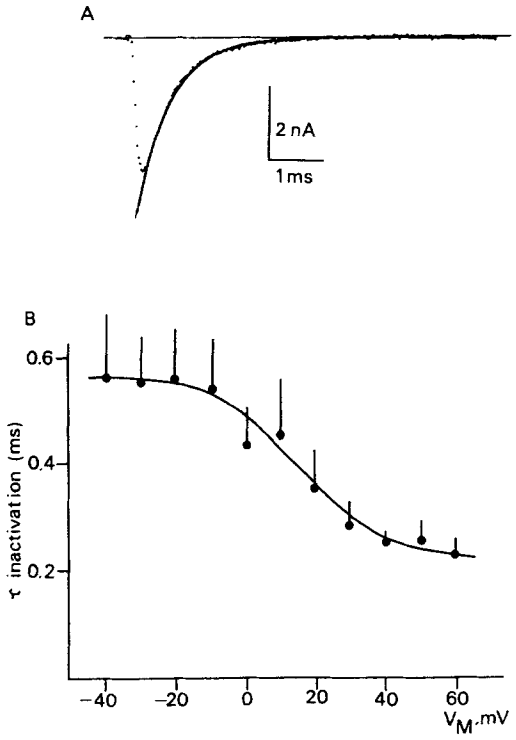

FIGURE 4. Time course of Na^+ current inactivation. (*A*) Single sweep of a Na^+ current recorded during a depolarization to 0 mV. A single exponential extrapolated to the onset of the pulse was fitted to inactivation time course. To facilitate comparison, the exponential is drawn superimposing the current trace. (*B*) Dependence of inactivation time constant on the pulse membrane potential. Circles are the mean and the bars the standard deviation of values from five cells. Solutions: Mg/Co//130 Cs.

shown that the amplitude of the current recorded by a test depolarization to 0 mV depends on the membrane potential during a conditioning prepulse lasting 50 ms. Fig. 5 *B* shows the relation between the noninactivated fraction of channels (ordinate) and the prepulse membrane potential (abscissa) with mean values obtained from six cells. At −80 mV only a small (5–10%) fraction of the channels are inactivated, but all of them are inactivated at voltages more positive than −20 mV. The average half steady-state inactivation occurs at a membrane potential of about −50 mV; this parameter varied between −45 and −70 mV in the cells studied.

Recovery from inactivation was studied by applying a 20-ms conditioning pulse to 0

mV to inactivate the Na^+ current and, after a variable time interval at the holding potential, applying a test pulse to open the channels already deinactivated. The traces of Fig. 6 *A* are Na^+ currents elicited by depolarization to 0 mV in the absence of prepulse (control) and 10, 25, and 900 ms after the prepulse; inactivation is almost completely removed in the course of 900 ms. In Fig. 6 *B* are shown the time courses of recovery from inactivation when the membrane potential during the interval is held at −80 (*circles*), −100 (*squares*), or −120 mV (*triangles*). Recovery is about six times faster at −120 mV than at −80 mV. Interestingly, at −80 mV the recovery of the last 15–20% of the current required as much as 900 ms. This indicates the presence of a fast inactivating component that recovers extremely slowly.

Closing kinetics. Closing kinetics of mammalian neuronal Na^+ channels have not been previously studied. We often obtained recordings where the fast Na^+ tail

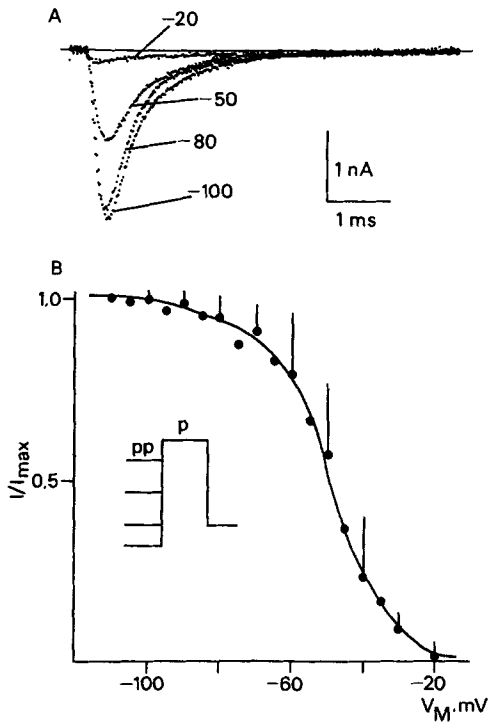

FIGURE 5. Steady-state inactivation of Na^+ currents. (*A*) Current sweeps during depolarizations to 0 mV preceded by a 50-ms prepulse to the indicated membrane potentials. Holding potential, −80 mV. Normalized fraction of peak current recorded during the pulse (ordinate) as a function of the prepulse membrane potential. Circles and bars are the mean and standard deviation values from five cells. The inset illustrates the pulse protocol. Solutions: Mg/Co//130 Cs.

currents could be resolved. The protocol consisted of the application of a brief depolarization (0.3–0.5 ms) to open Na^+ channels that ended at the time when the current was maximal (Fig. 7 *A*). At the instant of repolarization the driving force for Na^+ suddenly increases and thus a tail current is recorded. The decay of the tail reflects the progressive deactivation of the channels open during the pulse. In our experiments Na^+ tail currents were always well fitted by a single exponential function (Fig. 7 *B*), which at −80 mV had a time constant faster than 100 μs (n = 5).

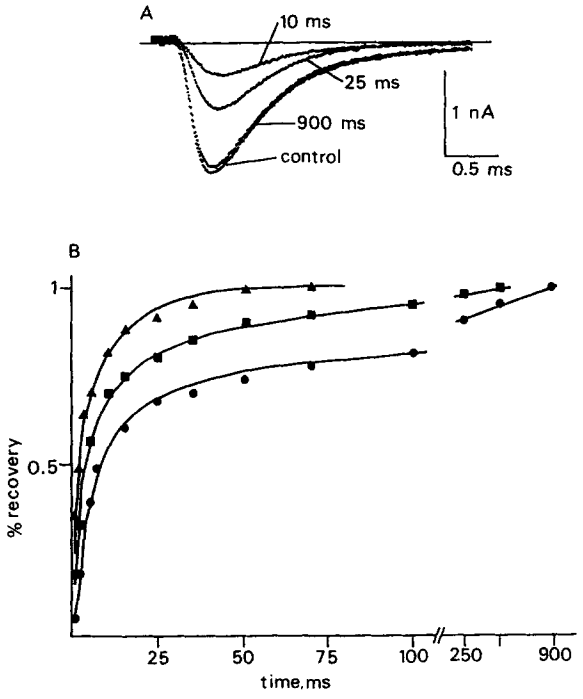

FIGURE 6. Recovery from inactivation of Na^+ channels. (*A*) Na^+ currents elicited by voltage steps to 0 mV at the indicated time intervals after a prepulse to 0 mV lasting 20 ms. The control trace was obtained in the absence of prepulse. Holding potential, −80 mV. (*B*) Normalized pulse current amplitude (ordinate) as a function of interval duration (abscissa). Membrane potentials during the prepulse were −80 mV (*circles*), −100 mV (*squares*), and −120 mV (*triangles*). Lines are fitted by eye. Solutions: Mg/Co// 130 Cs.

Ca^{2+} Channels

Identification and I-V relations. In the presence of TTX depolarization elicited in all neurons a slowly inactivating inward current that was readily identified as a Ca^{2+} current. Fig. 8*A* is a typical recording of the slow inward current. This trace shows that the current turns on slowly and almost reaches a maximum by the end of the 6-ms pulse. On repolarization there is a tail current due to the increase in the electrochemical gradient for Ca^{2+} ions. As in most preparations studied, the current was larger when Ba^{2+} ions instead of Ca^{2+} were used as charge carrier (Fig. 8 *B*). Current during the pulse and at the pulse end (tail) was suppressed after removal of

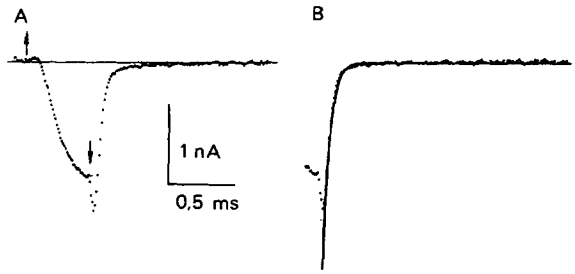

FIGURE 7. Closing kinetics of cerebral Na^+ channels. (*A*) Na^+ current recorded during a 0.5-ms voltage pulse (indicated between the arrows) to 0 mV from a holding potential of −80 mV. When the pulse is turned off a fast tail current is recorded. (*B*) Fitting of the deactivation time course by a single exponential with a time constant of 60 μs. The exponential is extrapolated to the instant of repolarization. Solutions: Mg/Co//130 Cs.

external Ca^{2+} for a mixture of Mg^{2+} and Co^{2+}, cations practically impermeant through Ca^{2+} channels (Fig. 8 *C*).

Fig. 9 shows a family of Ca^{2+} currents recorded on depolarization to the indicated membrane voltages. Current during the pulse, which is indicated between the arrows, increases in amplitude and activates more rapidly at more depolarized levels. After a maximum the pulse current diminishes with positive potentials due to the decrease in the electrochemical gradient for Ca^{2+}. Ca^{2+} current measured at the end of the 6-ms steps at various membrane potentials is illustrated in Fig. 10. This *I-V* curve shows that the current becomes detectable at −40 to −50 mV, reaches a maximum at about +20 mV, and afterwards declines as the driving force for Ca^{2+} progressively decreases. In 10 mM external Ca^{2+} the amplitude of the current measured at the end of 6-ms pulses to 20 mV was 0.35 ± 0.22 nA (n = 12).

Separation of two Ca^{2+} channel types. It is clearly seen in Fig. 9 that after small depolarizations the decay of the tails follows a simple, slow time course, but after depolarizations to potentials more positive than 0 mV a large fast component also

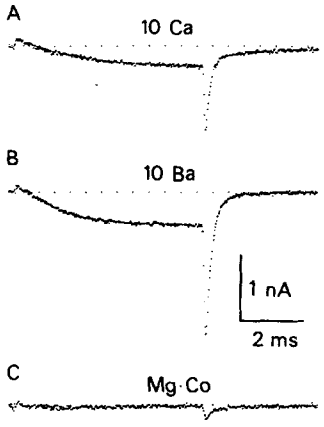

FIGURE 8. Identification of Ca^{2+} currents. (*A*) Current produced by depolarization to 10 mV during 6 ms with Ca^{2+} as charge carrier. (*B*) Current recorded in the same cell and with the same pulse, using Ba^{2+} instead of Ca^{2+} in the external solution. (*C*) Blockade of the current after replacement of Ca^{2+} by Mg^{2+} and Co^{2+}. Holding potential, −80 mV. The different external solutions are indicated in the figure; the internal solution was 130 Cs.

appears. Both the slow and fast components of the tails grow larger as the membrane potential is made more positive. The sudden appearance of the fast component of the tails at voltages between 0 and 20 mV parallels the sharp transition seen in the *I-V* curve at the same voltages (Fig. 10). These observations suggest the existence in septal neurons of at least two different Ca^{2+} conductances with different activation voltages and deactivation kinetics. These conductances are probably due to the activity of two kinds of Ca^{2+} channels.

Separation of the two components of the Ca^{2+} current was done following the method illustrated in Fig. 11 (Cota, 1986; Matteson and Armstrong, 1986; Tabares et al., 1989). Trace *A* is a tail current recorded on repolarization to −80 mV after a pulse to 40 mV lasting 6 ms. An exponential is fitted to the slow component and extrapolated back to the instant of repolarization. Subtraction of the slow exponential from the total current yields a fast component on isolation which could be fitted by another exponential with a faster time constant. Thus, each exponential function represents the closing time course of slow (SD) and fast (FD) deactivating Ca^{2+}

channels. At 25°C and with 10 mM external Ca^{2+} the closing time constants at −80 mV were 1.99 ± 0.2 ms (n = 6) for SD and 0.11 ± 0.03 (n = 6) ms for FD channels. Conductance–voltage relations for these channels can be studied plotting the normalized amplitude of each component of the tails as a function of the activation membrane potential. This is shown in Fig. 11 *C*, where it is clearly seen that SD channels (*circles*) begin to activate at membrane potentials between −50 and −40 mV and half-maximal conductance is obtained at 0 mV, whereas for FD channels (*squares*)

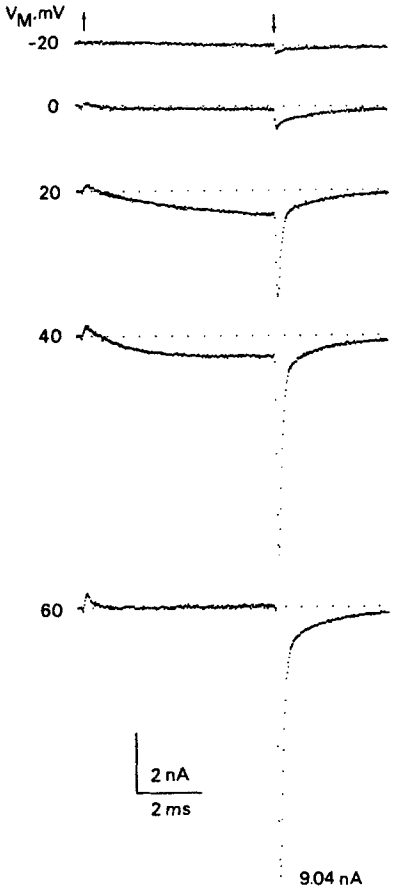

FIGURE 9. Ca^{2+} currents recorded by depolarization to the membrane potentials indicated on the left of each trace. Pulse duration (6 ms) is indicated between the arrows. Holding potential, −80 mV. Solutions: 10 Ca(TTX)//130 Cs.

the same parameters are −20 and 20 mV, respectively. In addition, the eye-fitted lines illustrate that the slope of the conductance–voltage curve for FD channels is greater than for SD channels.

Inactivation and wash-out. During a maintained depolarization the Ca^{2+} current partially inactivates (Fig. 12 *A*). Inactivation is, however, a process that affects SD and FD conductances unequally. Fig. 12, *B* and *C*, shows tail currents recorded after pulses to 20 mV lasting 10 and 100 ms. The two components of the tail are present at

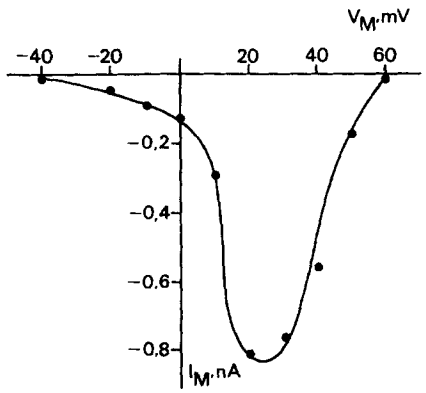

FIGURE 10. Ca^{2+} current amplitude measured at the end of 6-ms pulses (ordinate) as a function of the step membrane potential. The continuous line was fitted by eye. Solutions: 10 Ca (TTX)//130 Cs.

the repolarization of the shortest pulse (*B*), but after the 100-ms depolarization the slow component is drastically reduced while the fast component remains almost intact. Fig. 12 *D* plots the normalized amplitude of the slow (*circles*) and fast (*squares*) components of tail currents (ordinate) recorded at the repolarization of pulses of variable duration (abscissa). This figure reveals that after 100 ms ~60–70% of SD channels but only 5–10% of FD channels are inactivated. Thus, inactivation in SD channels is much faster than in FD channels, which inactivate very slowly.

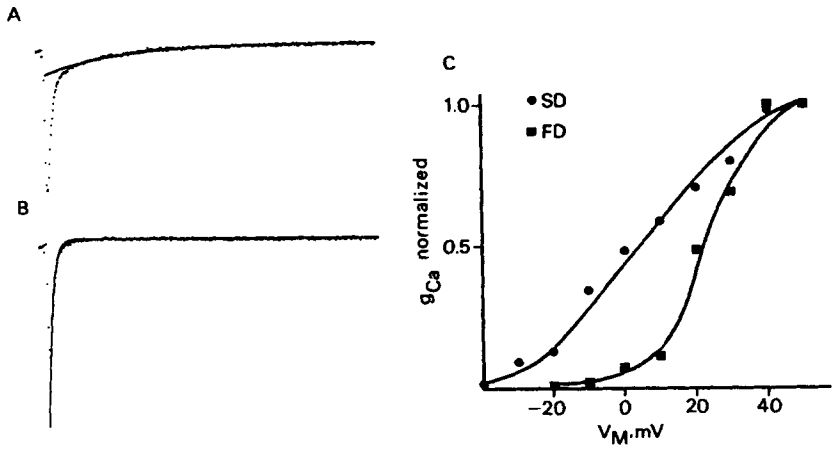

FIGURE 11. Separation of FD and SD Ca^{2+} channels. (*A*) Ca^{2+} tail current recorded on stepping back to −80 mV. The pulse voltage was 40 mV and the duration was 6 ms. A single exponential with a time constant of 1.96 ms fits the slow component of the deactivation current. The exponential is extrapolated to the instant of repolarization. (*B*) Subtraction of this exponential from the current trace gives a fast component that is fitted by a faster exponential (time constant, 0.15 ms). (*C*) Normalized amplitudes of fast and slow components of tails generated after depolarizations to various membrane potentials. The eye-fitted continuous lines are the conductance–voltage curves for SD and FD channels. Solutions: 10 Ca (TTX)//130 Cs.

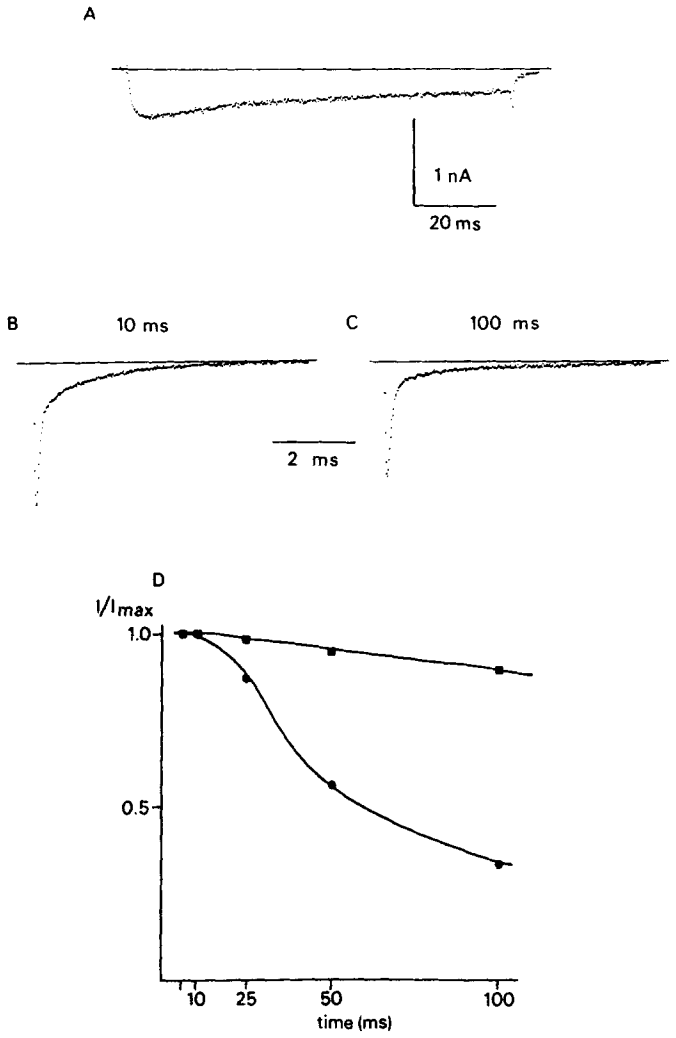

FIGURE 12. Inactivation of Ca^{2+} currents. (*A*) Partial inactivation of a Ca^{2+} current in the course of a depolarization to 20 mV for 90 ms. (*B* and *C*) Tail currents recorded after short (*B*) and long (*C*) lasting depolarizations. (*D*) Normalized amplitude of the slow (*circles*) and fast (*squares*) components of Ca^{2+} tails (ordinate) recorded at the repolarization of pulses of variable duration (abscissa). Pulse membrane potential was 60 mV. Solutions: 10 Ca (TTX)//130 Cs.

Besides their differences in inactivation time course, FD and SD channels also differ in their stability during intracellular dialysis. Fig. 13 shows two superimposed sweeps of Ca^{2+} current recorded 20 and 400 s from the initiation of the whole-cell recording mode. After 400 s of cell dialysis the fast component of the tail has almost disappeared but the slow component remains unaffected. This finding indicates that cerebral FD channels, similar to high voltage activated Ca^{2+} channels of other tissues

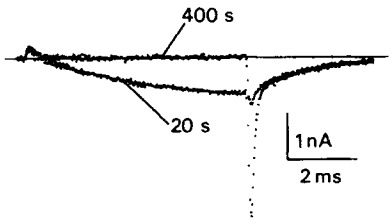

FIGURE 13. Wash-out of fast deactivating Ca^{2+} channels during intracellular dialysis. Superimposed Ca^{2+} current sweeps obtained by depolarization to 40 mV, 20 and 400 s after the onset of the whole-cell recording. Holding potential, −80 mV. Solutions: 10 Ca (TTX)//130 Cs.

(Forscher and Oxford, 1985; Cota, 1986; Ureña et al., 1989*a*) become nonfunctional as the whole-cell recording progresses, probably due to dilution of cytosolic components. As in other preparations (Forscher and Oxford, 1985; Cota, 1986), wash-out of FD channels was retarded by adding 3–4 mM Mg-ATP to the internal solution.

Variability in the components of the Ca^{2+} current. Although the two components of the Ca^{2+} tail current were observed in almost every dissociated septal neuron, there was a large variability in the relative contribution of each type of conductance to the total current. This could be explained by a variable distribution of Ca^{2+} channel types in different neuronal classes. In Fig. 14 Ca^{2+} tail currents recorded with the same experimental protocol in cells of similar size, clamp speed, and time after plating are shown. In Fig. 14 *A* the slow component is large and the fast component is almost absent.The opposite can be seen in *C*, where a large fast tail is present, and an intermediate situation is shown in trace *B*. In the total number of cells (n = 65) where Ca^{2+} tails were studied, the estimated proportion of FD and SD channels were, respectively, 73 and 27%. Only a few cells lacked FD channels, whereas SD channels where absent, or their contribution to the current almost negligible, in 15–20% of the neurons.

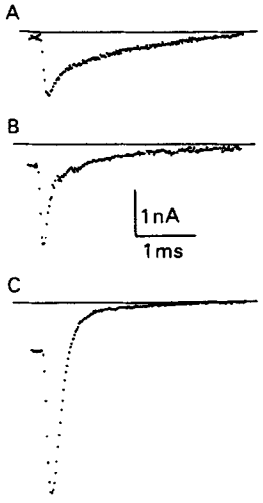

FIGURE 14. Variability in the contribution of FD and SD channels to the total Ca^{2+} current. The traces are tail currents generated at the end of pulses to 40 mV lasting 6 ms, recorded in three different septal neurons subjected to identical experimental conditions. Holding potential, −80 mV. Solutions: 10 Ca (TTX)//130 Cs.

DISCUSSION

Na^+ Conductance

Septal neurons exhibited large Na^+ currents with an average estimated density (0.6 mA cm^{-2}) that corresponds roughly to 5–10 channels/μm^2. Estimations in chromaffin (Fenwick et al., 1982) and hippocampal (Sah et al., 1988) cells are comparable to our own. In the soma of Purkinje cells (Gähwiler and Llano, 1989) Na^+ current density seems to be, however, larger than in septal neurons. Interestingly, in all central neurons so far studied Na^+ channel density is higher than in nonneuronal mammalian cells (Dubinsky and Oxford, 1984; Ureña et al., 1989*a*), but it is far from the 200–300 channels/μm^2 existing in the squid axon. The Na^+ current in septal neurons resembles the current in the squid axon and other preparations; it has fast activation and inactivation, is blocked by TTX, and is selectively carried by Na^+ ions. Na^+ current in the septum, as in hippocampal, Purkinje, and retinal ganglion cells (Sah et al., 1988; Barres et al., 1989; Gähwiler and Llano, 1989), activates at voltages more negative than in chromaffin (Fenwick et al., 1982), GH_3 (Fernández et al., 1984; Matteson and Armstrong, 1984), and glomus (Ureña et al., 1989*a*) cells. The neuronal *I-V* curves are, however, superimposable to the activation of rat brain Na^+ channel type II expressed in oocytes (Stühmer et al., 1987).

During a maintained depolarization Na^+ currents inactivate with an exponential time course. At all the membrane potentials studied inactivation was completed in $<$6–7 ms. A single exponential decay is found in the squid axon (Hodgkin and Huxley, 1952; Bezanilla and Armstrong, 1977), hippocampal neurons (Sah et al., 1988), and GH_3 and glomus cells (Vanderberg and Horn, 1984; Ureña et al., 1989*a*). On the contrary, it has been found that a double exponential is needed to fit inactivation time course in the vertebrate node of Ranvier (Chiu, 1977). Recent investigations in neocortical neurons (Huguenard et al., 1988) and Purkinje cells (Gähwiler and Llano, 1989) have revealed the presence of a slowly inactivating component in the Na^+ current. In these same preparations previous electrophysiological studies had suggested the existence of a persistent Na^+ conductance (Llinás and Sugimori, 1980; Stafstrom et al., 1985). This property was neither observed in the present study nor suggested by our own previous work in septal slices (Alvarez de Toledo and López-Barneo, 1988). Recovery from inactivation of Na^+ channels of central neurons has been studied only in neocortical (Huguenard et al., 1988) and hippocampal (Sah et al., 1988) cells. At the same membrane potentials, the recovery time constants in the septum were similar to those found in the neocortex of young animals, but about half as big as the measurements done in hippocampal cells. Recovery from inactivation in squid Na^+ channels is much faster even at a lower temperature (Bezanilla and Armstrong, 1977). We are not aware of the existence of previous reports on the closing kinetics of brain Na^+ channels. Here we show that at -80 mV their deactivation is very fast, with a time constant faster than 100 μs. By comparison, squid Na^+ channels close with a time constant of 150 μs at -70 mV and 8–10°C (Gilly and Armstrong, 1984).

Thus, there are quantitative dissimilarities among Na^+ channels from various preparations. These differences may be a result of the variability in the experimental

Published February 1, 1991

conditions (Sah et al., 1988), but they may also reflect a diversity of the Na^+ channel protein. This second possibility is particularly evident in the case of glomus cells (Ureña et al., 1989*a*) and septal neurons (this work), which were recorded in identical experimental situations. Differences in the biophysical properties of neuronal and glial Na^+ channels have also been recently reported (Barres et al., 1989). The molecular biology of nonneuronal Na^+ channels is not well known, but the existence of at least three distinct Na^+ channel mRNAs has been reported in the mammalian brain (Noda et al., 1986; Stühmer et al., 1987).

Ca^{2+} Conductances

After suppression of Na^+ conductance with TTX septal neurons displayed a Ca^{2+} current that, although varied in amplitude from cell to cell, was in all experiments much smaller than the Na^+ current. This current resembles I_{Ca} from other vertebrate cells in its time course, in the ability of Ba^{2+} to substitute for Ca^{2+} as charge carrier, and in its blockade by external divalent cations (Fenwick et al., 1982; Hagiwara and Ohmori, 1982). The biphasic decay of Ca^{2+} tail currents of septal neurons indicates the existence of two kinds of Ca^{2+} conductances, which are probably the result of two types of Ca^{2+} channels with different deactivation kinetics (slow and fast deactivating channels; Matteson and Armstrong, 1986; Tabares et al., 1989). FD channels close almost as fast as Na^+ channels, while deactivation of SD channels is ~15–20 times slower. In addition, FD and SD channels differ in their activation voltage, steepness of the conductance–voltage curve, inactivation time course, and resistance to dilution of cytosolic components. These channels share most of their properties with the low and high voltage activated channels (LVA and HVA, respectively) (Carbone and Lux, 1987) or the "T" and "L" channels (Fox et al., 1987) of sensory neurons. Evidence indicating the existence of LVA and HVA Ca^{2+} channels has also been found in other CNS neurons (Hernández-Cruz and Pape, 1989; Meyers and Barker, 1989; see also Llinás, 1988).

Based on previous work using intracellular recording techniques, it has been hypothesized that HVA channels could be located in the dendrites, whereas LVA channels might be preferentially distributed in the soma (Llinás, 1988). In some enzymatically dispersed neurons, as for example in hippocampal neurons (Yaari et al., 1987), only LVA channels are found after dissociation and HVA channels appear 1 or 2 d later. In our experiments the two types of Ca^{2+} conductances were recorded in cells only 2 h after plating, which suggests that in most septal cells FD and SD channels may coexist at or near the soma. This observation do not necessarily discard a differential distribution of Ca^{2+} channels, since the HVA type may be more densely packed in the dendrites that in the soma (Llinás, 1988; Hernández-Cruz and Pape, 1989).

Ionic Channels and Electrophysiology of Septal Cells

The ionic conductances described here explain the different firing patterns of septal neurons (Alvarez de Toledo and López-Barneo, 1988). The large Na^+ conductance is responsible for the generation of fast action potentials, whereas the two kinds of Ca^{2+} channels explain the appearance of high and low threshold Ca^{2+} spikes. The

transient activation of SD channels and their low activation voltage make some septal neurons capable of firing either tonically or in a burst mode, depending on the membrane potential of the cells (Alvarez de Toledo and López-Barneo, 1988). It is worth mentioning that our previous data already suggested that in some septal neurons a significant proportion of FD channels might be located near the soma. The characteristic slow, high threshold Ca^{2+} spikes of these cells appeared during small current injections, which is not a common finding in other CNS neurons, and it was relatively usual to obtain recordings where an initial Na^+ spike of small amplitude was followed by larger and broader Ca^{2+} action potentials. These, considered as presumptive intradendritic recordings (López-Barneo et al., 1985), were probably impalements placed in the region between the soma and the primary dendrites.

The authors wish to thank J. Toledo for his collaboration in some experiments.

This work was supported by the Dirección General de Investigación Científica y Técnica (grant PB-86-0250). Dr. Antonio Castellano is a fellow of FISss.

Original version received 20 February 1990 and accepted version received 22 August 1990.

REFERENCES

Alvarez de Toledo, G., and J. López-Barneo. 1988. Ionic basis of the differential neuronal activity of guinea-pig septal nucleus studied *in vitro*. *Journal of Physiology*. 396:399–415.

Barres, B. A., L. L. Chun, and D. P. Corey. 1989. Glial and neuronal forms of the voltage-dependent sodium channel: characteristics and cell-type distribution. *Neuron*. 2:1375–1388.

Bezanilla, F., and C. M. Armstrong. 1977. Inactivation of the sodium channel. I. Sodium current experiments. *Journal of General Physiology*. 70:549–566.

Carbone, E., and H. D. Lux. 1987. Kinetics and selectivity of a low-voltage-activated calcium current in chick and rat sensory neurons. *Journal of Physiology*. 386:547–570.

Chiu, S. Y. 1977. Inactivation of sodium channels: second order kinetics in myelinated nerve. *Journal of Physiology*. 273:573–596.

Cota, G. 1986. Calcium channel currents in pars intermedia cells of the rat pituitary gland. *Journal of General Physiology*. 88:83–105.

Dubinsky, J. M., and G. S. Oxford. 1984. Ionic currents in two strains of rat anterior pituitary tumor cells. *Journal of General Physiology*. 83:309–339.

Fedulova, S. A., P. G. Kostyuk, and N. S. Veselovsky. 1985. Two types of calcium channels in the somatic membrane of new born rat dorsal root ganglion neurons. *Journal of Physiology*. 359:431–446.

Fenwick, E. M., A. Marty, and E. Neher. 1982. Sodium and calcium channels in bovine chromaffin cells. *Journal of Physiology*. 331:599–635.

Fernández, J. M., A. P. Fox, and D. Krasne. 1984. Membrane patches and whole-cell membranes: a comparison of electrical properties in rat clonal pituitary (GH_3) cells. *Journal of Physiology*. 356:565–585.

Forscher, P., and G. S. Oxford. 1985. Modulation of calcium channels by norepinephrine in internally dialyzed avian sensory neurons. *Journal of General Physiology*. 85:743–763.

Fox, A. P., M. C. Nowycky, and R. W. Tsien. 1987. Kinetic and pharmacological properties distinguishing three types of calcium currents in chick sensory neurons. *Journal of Physiology*. 394:149–172.

Gähwiler, B. H., and I. Llano. 1989. Sodium and potassium conductances in somatic membranes of rat Purkinje cells from organotypic cerebellar cultures. *Journal of Physiology.* 417:105–122.

Gilly, W. F., and C. M. Armstrong. 1984. Threshold channels: a novel type of sodium channel in squid giant axon. *Nature.* 309:448–450.

Hagiwara, S., and H. Ohmori. 1982. Studies of calcium channels in rat clonal pituitary cells with patch electrode voltage-clamp. *Journal of Physiology.* 331:231–252.

Hamill, O. P., A. Marty, E. Neher, B. Sakmann, and F. Sigworth. 1981. Improved patch-clamp techniques for high-resolution current recording from cells and cell-free membrane patches. *Pflügers Archiv.* 391:85–100.

Hernández-Cruz, A., and H. C. Pape. 1989. Identification of two calcium currents in acutely dissociated neurons from the rat lateral geniculate nucleus. *Journal of Neurophysiology.* 61:1270–1283.

Hodgkin, A. L., and A. F. Huxley. 1952. A quantitative description of membrane current and its application to conduction and excitation in nerve. *Journal of Physiology.* 117:500–544.

Huguenard, J. R., O. P. Hamill, and D. A. Prince. 1988. Developmental changes in Na^+ conductances in rat neocortical neurons: appearance of a slowly inactivating component. *Journal of Neurophysiology.* 59:778–795.

Llinás, R. 1988. The intrinsic electrophysiological properties of mammalian neurons: insights into central nervous system function. *Science.* 242:1654–1664.

Llinás, R., and M. Sugimori. 1980. Electrophysiological properties of *in vitro* Purkinje cell somata in mammalian cerebellar slices. *Journal of Physiology.* 305:171–195.

López-Barneo, J., G. Alvarez de Toledo, and Y. Yarom. 1985. Electrophysiological properties of guinea-pig septal neurons. *Brain Research.* 347:358–362.

Matteson, D. R., and C. M. Armstrong. 1984. Na and Ca channels in a transformed line of anterior pituitary cells. *Journal of General Physiology.* 83:371–394.

Matteson, D. R., and C. M. Armstrong. 1986. Properties of two types of calcium channels in clonal pituitary cells. *Journal of General Physiology.* 81:161–182.

Meyers, D. E., and J. L. Barker. 1989. Whole-cell patch-clamp analysis of voltage-dependent calcium conductances in cultured embryonic rat hippocampal neurons. *Journal of Neurophysiology.* 61:467–477.

Noda, M., T. Ikeda, T. Kayano, H. Suzuki, H. Takeshima, M. Kurasaki, H. Takahashi, and S. Numa. 1986. Existence of distinct sodium channel messenger RNA's in rat brain. *Nature.* 320:188–192.

Sah, P., A. J. Gibb, and P. Gage. 1988. The sodium current underlying action potentials in guinea-pig hippocampal CA1 neurons. *Journal of General Physiology.* 91:373–398.

Sigworth, F. J. 1983. Electronic design of the patch-clamp *In* Single Channel Recording. B. Sakmann and E. Neher, editors. Plenum Publishing Corp., New York. 3–35.

Stafstrom, C. E., P. C. Schwindt, M. C. Chubb, and W. E. Crill. 1985. Properties of persistent sodium conductance and calcium conductance of layer V neurons from cat sensorimotor cortex *in vitro*. *Journal of Neurophysiology.* 53:153–170.

Stühmer, W., C. Methfessel, B. Sakmann, and S. Numa. 1987. Patch clamp characterization of sodium channels expressed from rat brain cDNA. *European Biophysics Journal.* 14:131–138.

Swandulla, D., and C. M. Armstrong. 1988. Fast-deactivating calcium channels in chick sensory neurons. *Journal of General Physiology.* 92:197–218.

Tabares, L., J. Ureña, and J. López-Barneo. 1989. Properties of calcium and potassium currents of clonal adrenocortical cells. *Journal of General Physiology.* 93:495–519.

Ureña, J., J. R. López-López, C. González, and J. López-Barneo. 1989*a*. Ionic currents in dispersed chemoreceptor cells of the mammalian carotid body. *Journal of General Physiology.* 93:979–999.

Ureña, J., J. C. Mateos, and J. López-Barneo. 1989*b*. Low-cost system for automated acquisition, display and analysis of transmembrane ionic currents. *Medical & Biological Engineering & Computing*. 27:94–98.

Vandenberg, C. A., and R. Horn. 1984. Inactivation viewed through single sodium channels. *Journal of General Physiology*. 84:535–564.

Yaari, Y., B. Hamon, and H. D. Lux. 1987. Development of two types of calcium channels in cultured mammalian hippocampal neurons. *Science*. 235:680–682.